

Molecular dynamics simulations of collision cascades in polycrystalline tungsten

Lixia Liu(刘丽霞), Mingxuan Jiang(蒋明璇), Ning Gao(高宁), Yangchun Chen(陈阳春), Wangyu Hu(胡望宇), and Hiuqiu Deng(邓辉球)

Citation: Chin. Phys. B, 2025, 34 (**4**): 046103. DOI: 10.1088/1674-1056/adb410
Journal homepage: http://cpb.iphy.ac.cn; http://iopscience.iop.org/cpb

What follows is a list of articles you may be interested in

Structural and transport properties of $(Mg,Fe)SiO_3$ at high temperature and high pressure

Shu Huang(黄澍), Zhiyang Xiang(向志洋), Shi He(何适), Luhan Yin(尹路寒), Shihe Zhang(张时赫), Chen Chen(陈晨), Kaihua He(何开华), and Cheng Lu(卢成)

Chin. Phys. B, 2025, 34 (**3**): 036102. DOI: 10.1088/1674-1056/ada759

Quasi-plastic deformation mechanisms and inverse Hall-Petch relationship in nanocrystalline boron carbide under compression

Zhen Yue(岳珍), Jun Li(李君), Lisheng Liu(刘立胜), and Hai Mei(梅海)

Chin. Phys. B, 2024, 33 (**8**): 086105. DOI: 10.1088/1674-1056/ad4989

Properties of radiation defects and threshold energy of displacement in zirconium hydride obtained by new deep-learning potential

Xi Wang(王玺), Meng Tang(唐孟), Ming-Xuan Jiang(蒋明璇), Yang-Chun Chen(陈阳春), Zhi-Xiao Liu(刘智骁), and Hui-Qiu Deng(邓辉球)

Chin. Phys. B, 2024, 33 (**7**): 076103. DOI: 10.1088/1674-1056/ad362b

Effect of Y element on atomic structure, glass forming ability, and magnetic properties of FeBC alloy

Jin-Hua Xiao(肖晋桦), Da-Wei Ding(丁大伟), Lin Li(李琳), Yi-Tao Sun(孙奕韬), Mao-Zhi Li(李茂枝), and Wei-Hua Wang(汪卫华)

Chin. Phys. B, 2024, 33 (**7**): 076101. DOI: 10.1088/1674-1056/ad3dd4

Influence of helium on the evolution of irradiation-induced defects in tungsten: An object kinetic Monte Carlo simulation

Peng-Wei Hou(侯鹏伟), Yu-Hao Li(李宇浩), Zhong-Zhu Li(李中柱), Li-Fang Wang(王丽芳), Xingyu Gao(高兴誉), Hong-Bo Zhou(周洪波), Haifeng Song(宋海峰), and Guang-Hong Lu(吕广宏)

Chin. Phys. B, 2021, 30 (**8**): 086108. DOI: 10.1088/1674-1056/abf7ac

---

Molecular dynamics simulations of collision cascades in polycrystalline tungsten

Lixia Liu(刘丽霞)[1,2], Mingxuan Jiang(蒋明璇)[3], Ning Gao(高宁)[4], Yangchun Chen(陈阳春)[2], Wangyu Hu(胡望宇)[2,†], and Hiuqiu Deng(邓辉球)[3,‡]

[1] *School of Physics, Suqian University, Suqian* 223800, *China*
[2] *College of Materials Science and Engineering, Hunan University, Changsha* 410082, *China*
[3] *School of Physics and Electronics, Hunan University, Changsha* 410082, *China*
[4] *Institute of Frontier and Interdisciplinarity Science, Shandong University, Qingdao* 266237, *China*

(Received 9 December 2024; revised manuscript received 26 January 2025; accepted manuscript online 8 February 2025)

Using molecular dynamics methods, simulations of collision cascades in polycrystalline tungsten (W) have been conducted in this study, including different primary-knock-on atom (PKA) directions, grain sizes, and PKA energies between 1 keV and 150 keV. The results indicate that a smaller grain size leads to more defects forming in grain boundary regions during cascade processes. The impact of high-energy PKA may cause a certain degree of distortion of the grain boundaries, which has a higher probability in systems with smaller grain sizes and becomes more pronounced as the PKA energy increases. The direction of PKA can affect the formation and diffusion pathways of defects. When the PKA direction is perpendicular to the grain boundary, defects preferentially form near the grain boundary regions; by contrast, defects are more inclined to form in the interior of the grains. These results are of great significance for comprehending the changes in the performance of polycrystalline W under the high-energy fusion environments and can provide theoretical guidance for further optimization and application of W-based plasma materials.

Keywords: collision cascades, molecular dynamics simulations, tungsten, polycrystalline

PACS: 61.80.–x, 61.82.Rx, 61.72.–y, 71.15.Pd

DOI: 10.1088/1674-1056/adb410 **CSTR:** 32038.14.CPB.adb410

1. Introduction

Tungsten (W) is considered a leading candidate for plasma-facing materials (PFMs) in high-temperature and high-load future fusion reactors because of its advantageous characteristics, including a high melting point, chemical stability, and favorable thermal properties, and so on.[1–6] However, the PFMs in fusion reactors inevitably face intense exposure to high-energy particles, which can lead to a reduction in the service performance and a decrease in lifespan, significantly affecting the safety and stability of the fusion reactor.[7–10] Therefore, in the absence of fusion neutron sources for experimental irradiation, conducting simulation studies on neutron irradiation for fusion reactor materials is essential and conducive for enhancing the understanding of the engineering microstructural evolution in W, and it carries both theoretical importance and practical implications.

Many studies have been conducted to understand the irradiation damage of W in fusion environments. Using Large-scale Atomic Molecular Massively Parallel Simulator (LAMMPS)[11] code, Setyawan *et al.*[12] performed the simulations of collision cascade at primary-knock-on atom (PKA) energies of 0.1 keV–100 keV and temperatures between 300 K and 2050 K in W. Their results showed that the number of Frankel pairs is significantly dependent on the PKA energies in the final state, whereas temperature has a minimal impact. Liu *et al.*[13] established a comprehensive database of W cascade simulations through molecular dynamics (MD) methods, analyzing the influence of PKA energies, directions and temperatures. They observed that at low PKA energies, PKA directions and temperatures have statistically minimal effects on the number of Frenkel pairs and defect clusters; meanwhile, the PKA direction may affect the probability of forming ⟨100⟩ dislocation loops and the generation of sub-cascades. Fu *et al.*[14] simulated collision cascades in W and W–rhenium (W–Re) alloys at PKA energies between 100 keV and 300 keV, finding that Re has a negligible effect on Frankel pairs and the cluster size of defects and inhibits the mobility of interstitial clusters and dislocation loops compared with pure W systems, suggesting a pinning effect of Re on dislocation loops. Zhang *et al.*[15] explored cascade simulations of W near grain boundaries at various temperatures and discovered that the number of vacancy defects is independent of temperature. However, these studies have mainly focused on neutron irradiation damage to single crystals (SC) W and the influence of typical irradiation defects on the microstructural evolution of materials.

The mechanical properties of materials can be signifi-

†Corresponding author. E-mail: wyuhu@hnu.edu.cn
‡Corresponding author. E-mail: hqdeng@hnu.edu.cn

© 2025 Chinese Physical Society and IOP Publishing Ltd. All rights, including for text and data mining, AI training, and similar technologies, are reserved.

cantly enhanced and improved when the grain size of polycrystals reaches the nanometer (nm) scale, which makes nanocrystalline (NC) materials attractive for engineering applications in various fields.[16–20] Many studies have been conducted on the irradiation damage of NC materials. Levo *et al.*[16] examined the radiation tolerance of NC multicomponent alloys and discovered that alloys can withstand a much higher dose of irradiation before the nano-crystallinity collapses compared to SC nickel (Ni). Using MD simulations, Gao *et al.*[17] analyzed the generation of defects and the primary damage state in NC silicon carbide (SiC) with average grain diameters between 5 nm and 21 nm. The results indicate that the production of defects within gains generally increases with the increase of grain size and the efficiency also increases. Ma *et al.*[19] reported significant differences in microstructural evolution pattern between NC and SC materials, and NC W demonstrates enhanced resistance to irradiation-induced swelling under thermal conditions compared with a SC material. Park *et al.*[21] conducted radiation damage simulations for both single- and nano-(poly) crystalline W via the MD method and observed that the recombination of SIAs and vacancies occurred more rapidly in the SC structure than in the NC structure at the maximum damage state. Above studies illustrate the significant role of polycrystalline structures in influencing the material properties and the evolution behavior of defects under irradiation conditions. Therefore, it is essential to conduct irradiation damage simulations in nanocrystalline W to qualitatively explore how the grain size, PKA direction and energy influence the distribution and evolution of defects during cascade processes. This is of great importance for understanding the changes in the properties of relevant structural materials under radiation damage.

In this work, we have established the models of nano-(poly) crystalline W with different grain sizes and then conducted series of cascades to explore the radiation damage behavior and microstructural evolution characteristics of NC W. Considering the PKA direction, energy, and grain size, we analyzed the formation and distribution of defects, defect clusters, and the microstructural evolution of defects in NC systems during cascade processes. The findings of this study not only can enhance the understanding of the microstructural dynamics of polycrystalline materials and can provide a valuable theoretical basis for optimizing and utilizing W-based materials in fusion reactors.

2. Models and methods

The NC W simulation cells were created using the commonly used Voronoi cell method, as illustrated in Fig. 1. According to this method, the single crystal model is initially completed, followed by the rotation of the single crystals using a given rotation matrix. The translation process was achieved through the Voronoi method, which is crucial for identifying the atoms belonging to the grains between pairs of single crystals. In addition, all three dimensions were employed periodic boundary conditions (PBCs). The positions of the Voronoi grain centers were determined by a random number method. The corresponding criteria were closely related to the number of grains (N) in the simulation cells.

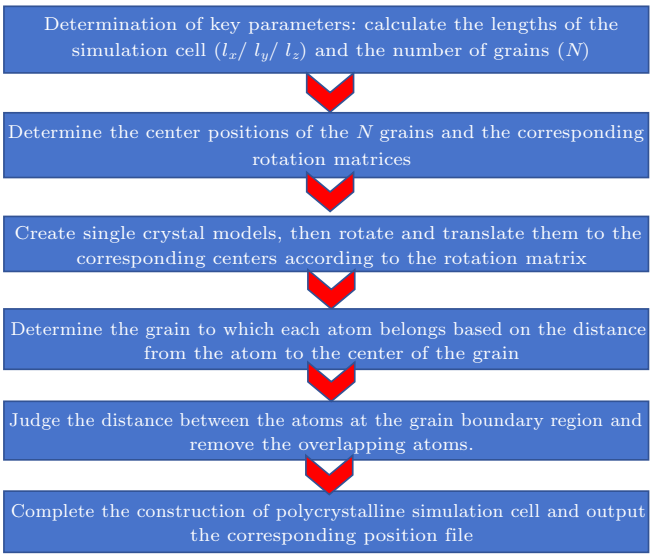


Fig. 1. Flowchart of the algorithm for constructing polycrystalline simulation cells based on the Voronoi method.

For instance, by giving the three lengths of the simulation cell (l_x, l_y, and l_z), the average size of each grain could be obtained the first-order approximation using either a cubic or spherical structure. Consequently, under the condition of a cubic structure, the average length (D) of each grain can be determined as follows:

$$D = \sqrt[3]{l_x l_y l_z / N}, \tag{1}$$

while under the approximation of a spherical structure, the radius length (R) of the spherical grains can be determined, they were denoted as

$$R = \sqrt[3]{3 l_x l_y l_z / 4\pi}. \tag{2}$$

Therefore, once the relevant key size parameters of the grains are determined, the center positions (P_i) of each grain can be obtained using a random number approach. For cubic structure grains, it can be assumed that the distance between each grain is not less than $2D$, while for spherical structure grains, it can be assumed that the distance between grains is not less than twice the diameter $2R$. It should be noted that this assumption is a first-order approximation, and based on this assumption, an NC W structure with a relatively uniform distribution of grain positions can be constructed.

After determining the corresponding positions of the grain centers P_i, the location of the perpendicular bisector plane between each pair of grain centers can be determined

using the Voronoi method. Ensure that all regions enclosed by P_i satisfy the range R determined by the following equation:

$$r_i \in \{x,y,z|d(r_i,P_i) < d(r_i,P_j)\},$$
$$j = \{1,2,\ldots,n\}, \quad j \neq i, \tag{3}$$

where r_i is the position vector, and $d(r_i,P_i)$ is the distance from the given position to the grain center. Therefore, based on the aforementioned equation, it becomes relatively easy to determine the grain to which a given position belongs, thereby achieving the initial establishment of the NC periodic structure.

As shown in Fig. 1, the grains are primarily constructed using rotation matrices. Based on the definition of grain boundary degrees of freedom, grains can be rotated at arbitrary angles around three principal axes, enabling free rotation in three-dimensional space and the construction of corresponding grain boundaries. By employing commonly used rotation matrices, such as rotating a given angle θ around the Z-axis, the corresponding rotation matrix can be obtained as follows:

$$R_z(\theta) = \begin{bmatrix} \cos\theta & -\sin\theta & 0 \\ \sin\theta & \cos\theta & 0 \\ 0 & 0 & 1 \end{bmatrix}, \tag{4}$$

therefore, when the whole grain can be rotated in three-dimensional space in three given directions by rotating the angles of α, β, and γ, a three-dimensional (3D) rotation matrix can be derived as

$$R(\hat{n},\theta) = \begin{pmatrix} \cos\alpha\cos\beta\cos\gamma - \sin\alpha\sin\gamma & -\cos\alpha\cos\beta\sin\gamma - \sin\alpha\cos\gamma & \cos\alpha\sin\beta \\ \sin\alpha\cos\beta\cos\gamma + \cos\alpha\sin\gamma & -\sin\alpha\cos\beta\sin\gamma + \cos\alpha\cos\gamma & \sin\alpha\sin\beta \\ -\sin\beta\cos\gamma & \sin\beta\sin\gamma & \cos\beta \end{pmatrix}. \tag{5}$$

Using the above algorithm, we established NC W simulation cells, as shown in Fig. 2.

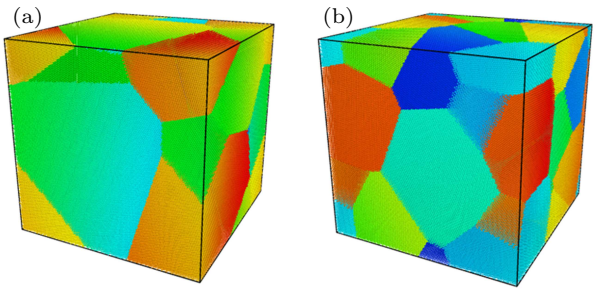


Fig. 2. Schematic structure of polycrystalline W: (a) the number of grains is 4 (4 grains) and (b) the number of grains is 12 (12 grains).

For better understanding the influence of grain size on cascade processes, two NC W systems were constructed in this study with simulation boxes of the same dimensions but containing different numbers of grains; that is, the grain size is different, as shown in Fig. 2. In Fig. 2(a), the number of grains in the simulation cells is 4 (4 grains), which contains 1993041 atoms, and the average grain size is 20.0 nm. As illustrated in Fig. 2(b), the simulation cell contains 12 grains (12 grains) with an average grain size of 13.9 nm and 1989660 atoms. Once the simulation models were established, to obtain the corresponding stable structures, molecular statics (MS) simulations were initially performed for relaxation, followed by MD simulations with a period of 30 picosecond (ps) for the dynamic equilibrium relaxation, which can provide a basis model for subsequent displacement cascade simulations.

To better compare with the relevant irradiation experiments of Hu *et al.*[22] and to establish a systematic database of W collision cascades with the previous work,[13] in this study, the cascade simulations of NC W were carried out at a temperature of 363 K, which provides the foundation for the effective connection and transfer of information between different simulation scales. The PKA energies (E_{PKA}) in the range of 10 keV–150 keV are considered. To adjust the atomic velocities at the target temperature, we utilized a Nose–Hoover thermostat[23] on a layer with a thickness of about 3 lattice units in the outermost part of the box. As indicated by previous research,[13,14,24–28] a microcanonical ensemble (NVE) and canonical ensemble (NVT) were applied to the interior and outermost atoms of the simulation box. Additionally, the distance between the PKA and the GB plane may affect the distribution of defects.[15] To ensure that collision cascades predominantly occurred in the core of the simulation box, the primary knock-on atom (PKA) is randomly selected within a distance of approximately five nanometers from the central grain boundary. The directions of the PKA (D_{PKA}) were examined in both perpendicular and parallel orientations with respect to the grain boundary. During the collision cascade processes, the time step was automatically varied from 10^{-3} ps to 10^{-7} ps, and the total simulation time for cascades was modified between 40 ps and 120 ps based on the PKA energy. Once an atom exceeds the boundaries of the simulation box, the simulation terminates immediately, and the data from that case is deemed invalid. Given the differences among individual cascades, each sample underwent over 20 cascades to obtain reliable statistical results. Table 1 lists the parameters of the average grain size, simulation box, and PKA energy for the different systems. Furthermore, according to previous studies,[29–32] we also focused on calculating defects in the bulk regions within grains in this work, excluding irregular atomic arrangements in grain boundary regions. The bulk region (grain interior) was defined as being over 7 Å away from grain boundary, which is considered to be the distance of interactions between the grain boundary and W interstitials, as indicated by previous work.[33]

Table 1. Lists the simulation parameters in the 4-grain and 12-grain systems, including E_{PKA}, number of atoms in the box (Atoms), size of the simulation box (Box), simulation time (Time), and the average grain size.

Systems	E_{PKA} (keV)	Atoms	Box (Å^3)	Time (ps)	Average grain size (nm)
4 grains	10/20/35/50/ 80/100/150	1993041	317.58×317.58×317.58	40 ∼ 120	20.0
12 grains	10/20/35/50/ 80/100/150	1989660	317.58×317.58×317.58	40 ∼ 120	13.9

In this work, the Finnis–Sinclair-type interatomic potentials[34] developed by our group were used. They can precisely predict the basic features and the energies of radiation-induced defects of W, demonstrating excellent agreement with experimental data or DFT calculations.[34,35] The predicted values for the lattice constant of W to be 3.1652 Å and the cohesion energy to be 8.9 eV, respectively. The most stable interstitial configuration of W is ⟨111⟩ W–W dumbbell with a formation energy of 9.46 eV,[34,35] vacancy formation energy is 3.54 eV,[34,35] and GB energy of Σ5(130) symmetric tilt GB for W with a value of 2.34 J/m^2.[33] This potential predicts correctly the 1/2 ⟨111⟩ interstitial loops are the most stable in bulk W,[34,35] which are in good agreement with DFT calculations or experimental data. Moreover, these potentials have been applied in radiation-damage simulations of SC W and W containing GB structures.[13,14,36] To accurately simulate the interactions between two atoms at a close distance during cascade processes, we integrated the pair interaction function of potentials with the Ziegler–Biersack–Littmark (ZBL) universal function[37] by a connection function with the corresponding parameters sourced from Ref. [35]. Additionally, the point defects produced during the cascade processes were analyzed and identified using the Wigner–Seitz (WS) cell method.[38] The common neighbor analysis (CNA) method[39] was employed to analyze the local crystal structures, distinguishing between body-centered cubic (BCC) structures in the internal grain regions, the grain boundary region (identified as "other" by CNA), and radiation-induced defects. Both methods were executed using the visualization and data analysis software OVITO (Open Visualization Tool).[40]

3. Results and discussion

3.1. Production and distribution of defects

Figure 3 illustrates the defect distributions in the system containing 12 grains for different PKA directions at $E_{\mathrm{PKA}} =$ 10 keV during the thermal peak stage and the final stage after cascades. The cascade quickly arrives at the maximum damage state, usually occurring within 1 ps. When the direction of PKA is parallel to the grain boundaries ($D_{\mathrm{PKA}} = P$), as depicted in Fig. 3(a), most defects do not cross the grain boundary region and remain within the grains at $E_{\mathrm{PKA}} = 10$ keV. Here, atoms are coloured based on their potential energies, and the corresponding colours are indicated in the colour bar. For clarity, we focus only on the grain boundary regions and defect atoms. Figure 3(b) presents the morphology of the local structure in the final stable stage, where the enlarged red atoms represent defect atoms, as analyzed by CNA methods,[39] and the white atom regions represent grain boundaries. Figure 3(c) provides a closer view of the defect atoms within the grains of Fig. 3(b), and the atoms are also coloured by their potential energies. After cascades, the number of interstitials remaining in the grain interiors is lower than that of vacancies, as shown in Fig. 3(c), indicating a preference for interstitials to be absorbed by the grain boundaries, which is consistent with previous work.[36,41,42] Similarly, figures 3(d) and 3(e) illustrate the distribution of defects when the direction of PKA is oriented perpendicularly to the grain boundaries ($D_{\mathrm{PKA}} = V$). Figure 3(d) shows the peak defect generation stage. It can be seen that there is a higher likelihood of defects crossing into the grain boundary regions when $D_{\mathrm{PKA}} = V$, subsequently allowing for a greater number of defects to be absorbed by the grain boundaries. The morphologies of the defects in the final stable stage are depicted in Figs. 3(e) and 3(f).

As illustrated in Figs. 3(a) and 3(d), it can be observed that, at $E_{\mathrm{PKA}} = 10$ keV, defects are predominantly generated within the grains, and most defects do not cross into the grain boundaries for both $D_{\mathrm{PKA}} = V$ and $D_{\mathrm{PKA}} = P$. It is particularly noteworthy that the probability of defects crossing into the grain boundaries is relatively higher for $D_{\mathrm{PKA}} = V$ than for $D_{\mathrm{PKA}} = P$. In the stable stage, vacancies are generally greater in the bulk regions of grains than interstitials. This means that interstitials are preferentially captured by grain boundaries during the cascade process, thereby inhibiting their annihilation and recombination with vacancies within the grains. To further understand the effect of PKA directions, a comparison is conducted between the cases of $D_{\mathrm{PKA}} = P$ as illustrated in Figs. 3(a)–3(c) and $D_{\mathrm{PKA}} = V$ as illustrated in Figs. 3(d)–3(e). It can be found that the overall number of defects is slightly lower in the case of $D_{\mathrm{PKA}} = V$ than in $D_{\mathrm{PKA}} = P$. This phenomenon may be attributed to a more significant overlap region between the grain boundaries and cascade regions in the case of $D_{\mathrm{PKA}} = V$, facilitating the capture of more defects by the grain boundaries, which is consistent with previous work.[15,36] As a result, the number of defects within the grain interior is slightly lower for $D_{\mathrm{PKA}} = V$ as compared to $D_{\mathrm{PKA}} = P$, and the distribution of defects is influenced by the extent of overlap between the cascade centers and grain

boundaries.

Moreover, as illustrated in Fig. 4, we compared the defect distributions at the thermal peak stage of defect generation and the final stable stage of residual defects for two different grain sizes, namely, the systems contain 4 grains and 12 grains, as an example of $E_{\mathrm{PKA}} = 50$ keV and the direction of PKA is oriented perpendicularly to the grain boundaries. The results indicate that at $E_{\mathrm{PKA}} = 50$ keV, defects in both the 4-grain and 12-grain systems tend to migrate across the neighboring grain boundaries at the peak defect generation stage. As shown in Figs. 4(a) and 4(c), since the 12-grain system contains more grain boundaries than the 4-grain system, a greater number of defects generated during the thermal spike stage of the cascade process can cross the grain boundaries in the 12-grain systems, indicating a greater overlap between the cascades and the grain boundary regions. Consequently, as illustrated in Figs. 4(b) and 4(d), a significant number of defects are rapidly absorbed by the grain boundary regions, resulting in a lower number of defects remaining in the grain interiors of the 12-grain system compared to the 4-grain system. It is worth mentioning that interstitial-type defects in NC systems are also preferentially captured by grain boundaries, thereby leaving predominantly vacancy-type defects in the interior of grains, which is consistent with previous studies.[15,36,43] Furthermore, a comparison of Figs. 3 and 4 reveals that the probability of defects crossing into grain boundaries during the thermal peak stage increases as the PKA energy increases.

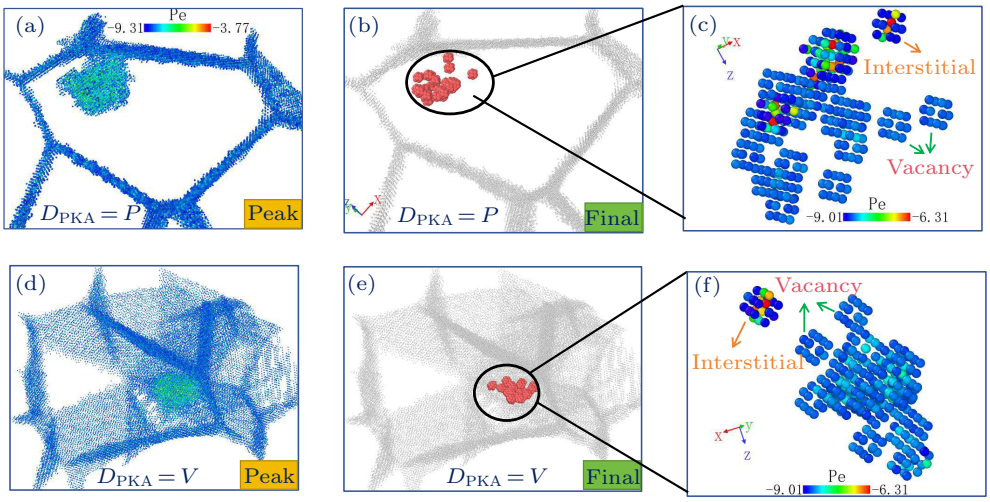


Fig. 3. Defect configurations after cascades in the systems containing 12 grains when the direction of PKA is parallel ($D_{\mathrm{PKA}} = P$) or perpendicular ($D_{\mathrm{PKA}} = V$) to the grain boundaries. (a) $D_{\mathrm{PKA}} = P$at the peak stage, (b) $D_{\mathrm{PKA}} = P$ at the final stage; (c) enlarged defects within the grains of panel (b); (d) $D_{\mathrm{PKA}} = V$ at the peak stage; (e) $D_{\mathrm{PKA}} = V$ at the final stage; (f) enlarged defects within the grains of panel (e). The atoms are coloured in terms of their potential energy. The red and enlarged balls in panels (b) and (e) represent defects, and the white atoms are grain boundaries.

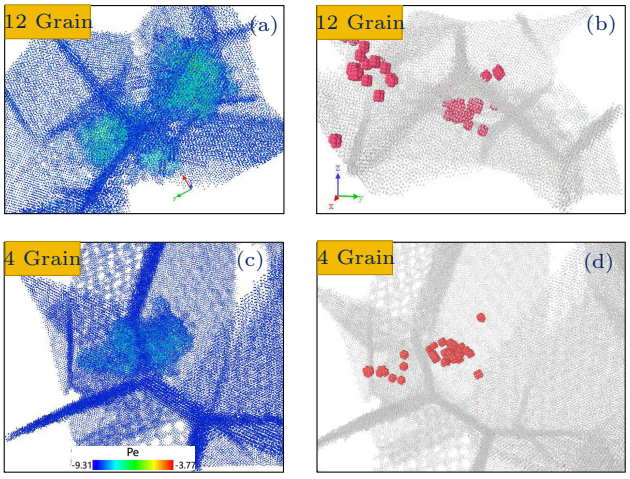


Fig. 4. Distribution of defect configurations for different grain size systems with $E_{\mathrm{PKA}} = 50$ keV and PKA direction is perpendicular to the grain boundaries as an example. (a) Peak stage of the system containing 12 grains; (b) final stage of the 12-grain system; (c) peak stage of the system containing 4 grains; (d) final stage of the 4-grain system. The atoms in panels (a) and (c) are coloured in terms of potential energy. The red and enlarged balls in panels (b) and (d) represent defects, and the white atoms are grain boundaries.

3.2. Defects and defect clusters

As depicted in Figs. 5(a) and 5(b), the number of surviving defects in the stable stage varies with PKA energies of 10 keV–150 keV for $D_{\mathrm{PKA}} = P$ and $D_{\mathrm{PKA}} = V$, respectively. It can be observed that both in the 4-grain and 12-grain systems, the number of vacancies (vac) in the interior bulk of grains is significantly greater than that of interstitials (int), and the number of interstitials in the grain interiors can be negligible at PKA energies below 50 keV, which is in alignment with previous research.[36,41,42] The strong absorption of interstitials in the grain boundary regions leads to a substantially higher number of vacancies remaining in the bulk region. As the PKA energy increases, the total number of defects exhibits a consistent increasing trend, in line with previous results for SC W.[13,14] Additionally, the number of grain boundaries impacted by the cascades in the thermal peak stage and the corresponding number of defects captured by grain boundary regions also exhibit significant increases with increasing PKA energy.

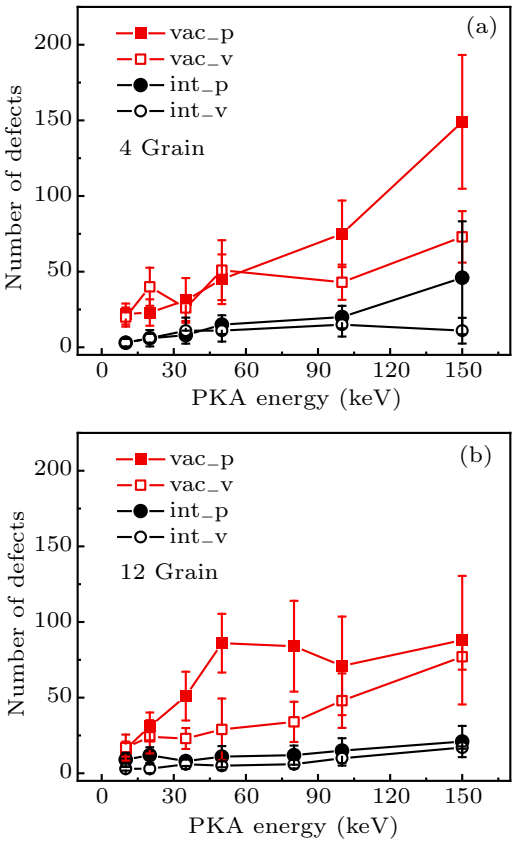


Fig. 5. Surviving defects after cascades with different PKA energies: (a) the system containing 4 grains and (b) the system containing 12 grains, respectively. Here, vac_p represents the number of vacancy obtained with the PKA direction parallel to the grain boundaries; vac_v represents the number of vacancy obtained with the PKA direction perpendicular to the grain boundaries; int_p represents the number of interstitial obtained with the PKA direction parallel to the grain boundaries; and int_v represents the number of interstitial obtained with the PKA direction perpendicular to the grain boundaries.

Figure 5 reveals that the direction of PKA may influence the distribution of defects, and more defects remain in the bulk region at the stable stage for the case of $D_{\mathrm{PKA}} = P$ compared to $D_{\mathrm{PKA}} = V$. This trend can be attributed to the fact that when $D_{\mathrm{PKA}} = P$, the majority of defects are generated in the interior of grains without crossing grain boundaries, where defects do not sufficiently interact with grain boundaries, leading to a higher number of residual defects in the interior of grains. A comparison of Figs. 5(a) and 5(b) shows that there are fewer surviving defects after cascades in the 12-grain system than in the 4-grain system. Specifically, for a fixed simulation box size, an increase in the number of grains corresponds to a decrease in the number of surviving defects in the interior of the grains. That is, as the grain size decreases, the number of surviving defects in the interior of the grains also diminishes. This phenomenon may be related to the higher number of grain boundaries present in systems with more grains, facilitating a more pronounced and rapid absorption of defects by grain boundaries, which is in good agreement with the findings of a previous study conducted by Gao *et al.*[17]

Upon comparing the number of defects obtained by the NC W system illustrated in Fig. 5 with the results obtained from the SC W system presented in Table 2 of previous work,[13] it is evident that the number of surviving defects in the NC system is fewer than that of the SC system in terms of both vacancies and interstitials. This observation demonstrates that, during cascading process, grain boundaries effectively capture a considerable number of interstitials and vacancies. However, the strong interaction between interstitials and grain boundaries leads to a preferential absorption of interstitials. Thus, a lower number of interstitials remain in the bulk (inside the grains) of the NC system compared to the SC system. At the same time, in the NC system, the number of interstitials absorbed by the grain boundaries exceeds that of vacancies, which hinders the annihilation or combination of many vacancies with interstitials. Consequently, these vacancies persist in the form of point defects or defect clusters in the interior of grains.

Table 2. Numbers of Frenkel pairs (FPs), the largest vacancy (S_{vac}) and the average number of vacancy cluster (N_{vac}) produced by single crystal (SC) W and NC W systems at 363 K. The data of SC W were obtained from the previous study.[13] Values in parentheses indicate standard deviations.

E_{PKA} (keV)	FPs	S_{vac}		N_{vac}	
	SC	SC	NC	SC	NC
10	17(5)	9	10	–	–
20	25(8)	9	13	1	2
35	41(12)	13	26	2	2
50	58(15)	23	43	4	3
80	101(31)	133	42	8	3
100	124(39)	107	43	11	4
150	235(113)	549	46	14	5

Based on the above results, we focused only on the statistical distribution of vacancy clusters in NC systems. Many previous studies[14,30,36,44–47] applied a cutoff distance criterion for vacancy clusters defined by the second nearest neighbor (NN2). The results of the radial distribution function $g(r)$ of vacancy defects obtained from the potentials[44] showed that the main peak appears at the second nearest neighbor. Thus, in this work, a vacancy was also classified as part of a cluster if it was within the NN2 range of another vacancy, and we considered two or more vacancies as a cluster. Figures 6 and 7 display the number and size distributions of vacancy clusters in the 4-grain and 12-grain systems, respectively, under different PKA energies and directions. We find that most vacancies remain point defect states in all NC systems, and small-sized clusters (≤ 10 net defects) dominate all simulations. In addition, there are more defect clusters when $D_{\mathrm{PKA}} = P$ than when $D_{\mathrm{PKA}} = V$ for both the 4-grain and 12-grain systems, especially in the case of cluster size > 10. As shown in Fig. 6, the size of vacancy clusters is dominated by < 10 in the 4-grain system, and the number of vacancy clusters increases with the increase of PKA energy. Comparing Figs. 6(a) and 6(b), it can be seen that the number and size

distribution of vacancy clusters are more for $D_{\mathrm{PKA}} = P$ than for $D_{\mathrm{PKA}} = V$, especially in the case of cluster size > 10. In fact, the size of vacancy clusters exceeding 10 was rarely observed when $D_{\mathrm{PKA}} = V$ because of the sufficient interaction between defects and grain boundaries and most defects captured by sinks. The largest vacancy cluster obtained from the 4-grain system consists of 34 vacancies, occurring at a PKA energy of 150 keV when the direction of PKA is parallel to the grain boundaries. The results of the 12-grain system in Fig. 7 are similar to those of the 4-grain system. Interestingly, even though the total number of vacancies in the interior of grains is lower in the 12-grain system compared to the 4-grain system, the 12-grain system demonstrates a higher number of vacancy clusters. This indicates that systems with more grains are more likely to form vacancy clusters. The relatively large-size clusters (> 10) are greater in the 12-grain system than in the 4-grain system, as shown in Fig. 7, and the largest vacancy cluster obtained from the 12-grain system includes 46 vacancies, occurring at a PKA energy of 150 keV when the direction of PKA is parallel to the grain boundaries. When the PKA energy is lower than 50 keV, the difference of the largest vacancy (S_{vac}) between the NC and SC systems is small, as shown in Table 2. However, when the PKA energy is larger than 50 keV, the largest vacancy in NC systems is much lower than that in SC systems. For example, the largest vacancy contains 46 vacancies under a PKA energy of 150 keV in NC systems, which contains 549 vacancies in SC systems.[13] This means that a relatively large number of defects aggregate at grain boundaries in the high energy PKA cascades, which may affect the evolution of defects and the mechanical properties of the materials. Moreover, numbers of vacancy cluster (N_{vac}) produced by SC systems are also greater than in NC systems, and small-sized vacancy clusters (≤ 10 net defects) dominate in NC systems. The comparison between Figs. 6 and 7 reveals that, overall, the number of larger-sized vacancy clusters is higher in the 12-grain system than in the 4-grain system, and the direction of PKA may affect the size of vacancy clusters. Specifically, there is a higher possibility of producing larger vacancy clusters when the direction of PKA is parallel to the grain boundaries.

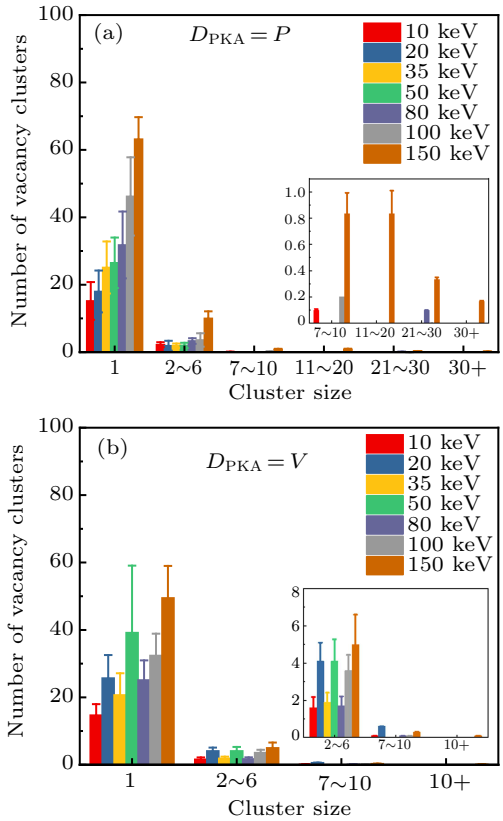


Fig. 6. The number and size distribution of vacancy clusters for the system containing 4 grains: (a) the direction of PKA is parallel to the grain boundaries ($D_{\mathrm{PKA}} = P$) and (b) the direction of PKA is perpendicular to the grain boundaries ($D_{\mathrm{PKA}} = V$). The standard deviation of the mean is shown by bars.

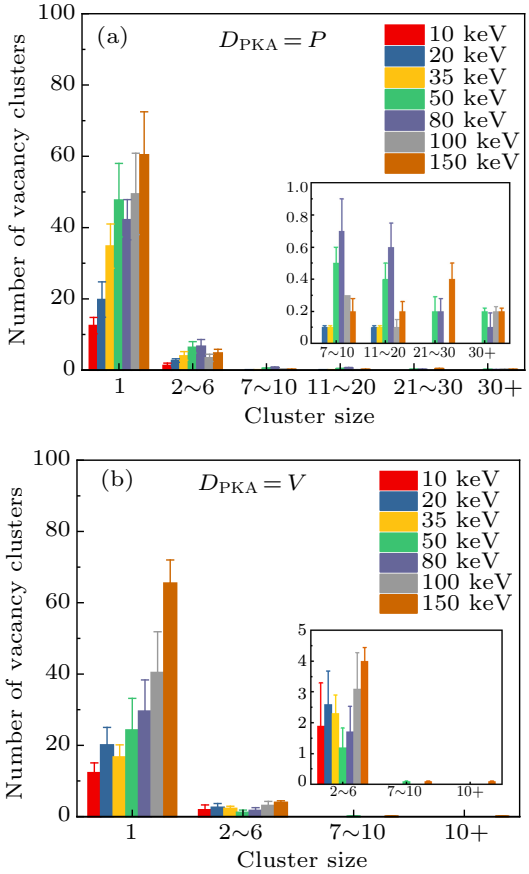


Fig. 7. The number and size distributions of vacancy clusters in different PKA directions for the systems containing 12 grains: (a) $D_{\mathrm{PKA}} = P$ and (b) $D_{\mathrm{PKA}} = V$, respectively. The standard deviation of the mean is shown by bars.

3.3. Evolution of the grain boundary

Figure 8 shows the defect evolution of NC W during high-energy PKA cascades. Here, we take the system containing 4 grains at $E_{\mathrm{PKA}} = 100$ keV when the direction of PKA is parallel to the grain boundaries as an example. The initial configuration after relaxation is depicted in Fig. 8(a), where

the atoms in the grain boundary regions display an ordered arrangement. The first stage of the collision cascade is depicted in Fig. 8(b), and the system quickly enters a thermal spike state within 1 ps, as illustrated in Fig. 8(c). As the cascade progresses, the system proceeds to the quenching stage, as shown in Fig. 8(d). Interstitials and vacancies begin to annihilate and combine, and defects near the grain boundary regions are rapidly absorbed by the grain boundary regions, particularly interstitial-type defects. Finally, a snapshot of the stable stage configuration is shown in Fig. 8(e), where most interstitial-type defects are absorbed into grain boundary regions, resulting in a higher concentration of vacancy-type defects in the interior of grains. Due to the significant absorption of a large number of interstitials and the intense impact from the cascades, grain boundaries undergo a certain degree of distortion, as represented in Fig. 8(f). Moreover, by comparing the width of the grain boundary at the stable stage in Fig. 8(e) with that at the initial stage in Fig. 8(a), it can be seen that the width of the grain boundary expands following the cascade. This phenomenon suggests that a significant number of defects are absorbed by the adjacent grain boundary regions, causing some migration and growth of grain boundaries, which may affect the performance of materials under actual service conditions.

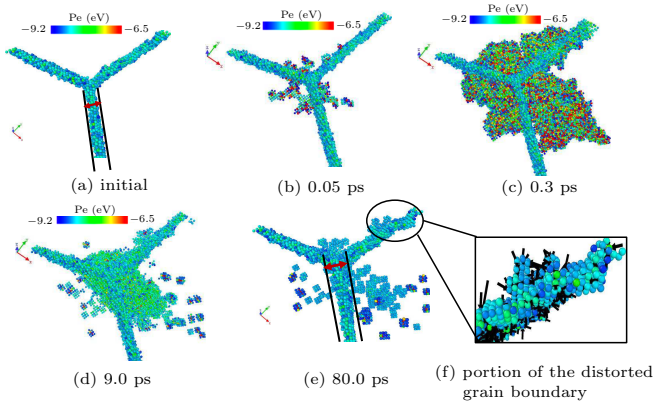


Fig. 8. Evolution snapshots of grain boundaries in NC W during high-energy PKA cascades (the system containing 4 grains as an example). (a) The initial model after relaxation, and a PKA possessing the energy of 100 keV was oriented parallel to the grain boundary to start the cascade. This process can be divided into the following stages: (b) initial stage, (c) peak stage, (d) quenching, (e) stable stage, and (f) enlarged portion of the distorted grain boundary region. Atoms are coloured according to their potential energy.

In addition, we find that the grain size has an impact on the distribution and evolution of defects during cascades. In the 12-grain system, which has smaller grain sizes, a greater number of defects formed in the grain boundary regions after cascades, resulting in a slightly higher distortion of the grain boundaries compared to the 4-grain system. This may be related to the lower diffusion barrier for defects near the grain boundary regions.[33] With a higher density of grain boundaries, the 12-grain system absorbs more defects, resulting in the greater distortion of grain boundaries than in the 4-grain system. Furthermore, the PKA direction may have an effect on the formation and diffusion pathways of defects. Defects tend to form near the grain boundary regions when the direction of PKA is oriented perpendicularly to the grain boundaries, whereas they have a higher probability of remaining in the interior of the grains when the direction of PKA is parallel to the grain boundaries. The PKA energy also significantly influences the formation and evolution of defects. Higher PKA energies result in an increased in defect formation coupled with accelerated defect diffusion rates, providing sufficient conditions to overcome the binding forces present within the crystal structure.

It is worth noting that, in this work, the interstitial dislocation loops and C15 clusters were hardly visible in NC systems, whereas the nucleation of interstitial loops and C15 clusters is easily observed in the SC W cascades, especially in high energy PKA.[13] This may be related to the complex stress fields and defect environments of NC materials, where the defect generation pattern may be more favorable to the formation of point defects than dislocation loops. Sinks present in the form of grain boundaries in NC materials have a significant effect on the mechanism of radiation-induced defects motion, influencing their dynamic behavior, and may change the microstructure and mechanical properties of materials.

4. Conclusion

This study systematically investigated the influence of grain size, the direction, and energy of PKA during the cascade process in NC W systems via MD simulations. We have analyzed the generation and distribution of defects, number, and type of defects/defect clusters, and the microstructure evolution of grain boundaries. These results can provide information for understanding the changes in the properties of the relevant structural materials under radiation damage. The main findings of this study can be summarized as follows.

(i) Vacancies dominating the defects in the interior of grains, and the number of defects increases as PKA energy increased.

(ii) As the number of grains increases, corresponding to a decrease in grain size, fewer defects are observed in the interiors of grains during the stable state, indicating greater absorption by the grain boundaries.

(iii) The PKA direction has an effect on the formation and diffusion pathways of defects. When PKA is perpendicular to the grain boundary, an increased number of defects is more likely to be absorbed by the grain boundaries, whereas a parallel incidence of PKA results in more defects forming in the interior of grains.

(iv) The impact of high energy PKA may induce noticeable distortion and even migration of grain boundaries.

Acknowledgements

Project supported by the National MCF Energy Research and Development Program of China (Grant No. 2018YFE0308101), the National Key Research and Development Program of China (Grant No. 2018YFB0704000), the Suqian Science and Technology Program (Grant No. K202337), and the Natural Science Foundation of the Jiangsu Higher Education Institutions of China (Grant No. 23KJD490001).

References

[1] Zhuang G, Li G Q, Li J, Wan Y X, Liu Y, Wang X L, Song Y T, Chan V, Yang Q W, Wan B N, Duan X R, Fu P and Xiao B J 2019 *Nucl. Fusion* **59** 112010

[2] Linsmeier Ch, Rieth M, Aktaa J, Chikada T, Hoffmann A, Hoffmann J, Houben A, Kurishita H, Jin X, Li M, Litnovsky A, Matsuo S, von Müller A, Nikolic V, Palacios T, Pippan R, Qu D, Reiser J, Riesch J, Shikama T, Stieglitz R, Weber T, Wurster S, You J H and Zhou Z 2017 *Nucl. Fusion* **57** 092007

[3] Knaster J, Moeslang A and Muroga T 2016 *Nat. Phys.* **12** 424

[4] Wittlich K, Hirai T, Compan J, Klimov N, Linke J, Loarte A, Merola M, Pintsuk G, Podkovyrov V, Singheiser L and Zhitlukhin A 2009 *Fusion Eng. Des.* **84** 1982

[5] Wang J, Li C, Yuan Y, Greuner H, Cheng L and Lu G H 2018 *Nucl. Fusion* **58** 096001

[6] Li X, Wang Y, Zhang Y, Xu Y, Li X, Wang X, Fang Q, Wu X and Liu C S 2022 *J. Nucl. Mater.* **563** 153637

[7] Ipatova I, Harrison R W, Donnelly S E, Rushton M J D, Middleburgh S C and Jimenez-Melero E 2019 *J. Nucl. Mater.* **526** 151730

[8] Yi X, Arakawa K, Du Y, Ferroni F, Han W, Liu P and Wan F 2019 *Nucl. Mater. Energy* **18** 93

[9] Qiu R, Chen Y, Liu L, Liu Z, Gao N, Hu W and Deng H 2021 *J. Nucl. Mater.* **556** 153162

[10] Jiang L, Li M, Fu B, Cui J and Hou Q 2024 *Chin. Phys. B* **33** 036103

[11] Plimpton S 1995 *J. Comput. Phys.* **117** 1

[12] Setyawan W, Nandipati G, Roche K J, Heinisch H L, Wirth B D and Kurtz R J 2015 *J. Nucl. Mater.* **462** 329

[13] Liu L, Qiu R, Chen Y, Jiang M, Gao N, Huang B, Gao F, Hu W and Deng H 2023 *J. Nucl. Mater.* **580** 154415

[14] Fu J, Chen Y, Fang J, Gao N, Hu W, Jiang C, Zhou H B, Lu G H, Gao F and Deng H 2019 *J. Nucl. Mater.* **524** 9

[15] Zhang C G, Zhou W H, Li Y G, Zeng Z and Ju X 2015 *J. Nucl. Mater.* **458** 138

[16] Levo E, Granberg F, Utt D, Albe K, Nordlund K and Djurabekova F 2019 *J. Mater. Res.* **34** 854

[17] Gao F, Chen D, Hu W and Weber W J 2010 *Phys. Rev. B* **81** 184101

[18] Samaras M, Derlet P M, Van Swygenhoven H and Victoria M 2003 *J. Nucl. Mater.* **323** 213

[19] Ma P W, Mason D R, Van Boxel S and Dudarev S L 2024 *Phys. Rev. Mater.* **8** 083601

[20] Du J 2009 in *AIP Conference Proceedings: American Institute of Physics* **1099** 981

[21] Park N Y, Cha P R, Kim Y C, Seok H K, Han S H, Lee S C, Cho S and Jung H 2009 *Met. Mater. Int.* **15** 447

[22] Hu X, Koyanagi T, Fukuda M, Kumar N K, Snead L L, Wirth B D and Katoh Y 2016 *J. Nucl. Mater.* **480** 235

[23] Martyna G J, Klein M L and Tuckerman M 1992 *J. Chem. Phys.* **97** 2635

[24] Lin Y, Yang T, Lang L, Shan C, Deng H, Hu W and Gao F 2020 *Acta Mater.* **196** 133

[25] Shan C, Lang L, Yang T, Lin Y, Gao F, Deng H and Hu W 2020 *Comp. Mater. Sci.* **177** 109555

[26] Liu L, Gao N, Chen Y, Qiu R, Hu W, Gao F and Deng H 2021 *Phys. Rev. Mater.* **5** 093605

[27] Xia Y, Wang Z, Wang L, Chen Y, Liu Z, Wang Q, Wu L and Deng H 2022 *Metals* **12** 763

[28] Peng Q, Meng F, Yang Y, Lu C, Deng H, Wang L, De S and Gao F 2018 *Nat. Commun.* **9** 1

[29] Yu Y, Shu X, Liu Y, Niu L, Jin S, Gao F and Lu G H 2015 *Sci. China-Phys. Mech.* **58** 1

[30] Li X, Liu W, Xu Y, Liu C S, Pan B C, Liang Y, Fang Q F, Chen J L, Luo G N, Lu G H and Wang Z 2016 *Acta Mater.* **109** 115

[31] Li X, Liu W, Xu Y, Liu C S, Pan B C, Liang Y, Fang Q F, Chen J L, Luo G N, Lu G H and Wang Z 2016 *Data Brief* **7** 798

[32] Chen Y, Li Y H, Gao N, Zhou H B, Hu W, Lu G H, Gao F and Deng H 2018 *J. Nucl. Mater.* **502** 141

[33] Liu L, Chen Y, Gao N, Hu W, Xiao S, Gao F and Deng H 2020 *Comput. Mater. Sci.* **173** 109412

[34] Chen Y, Fang J, Liu L, Hu W, Jiang C, Gao N, Zhou H B, Lu G H, Gao F and Deng H 2019 *J. Nucl. Mater.* **522** 200

[35] Liu L, Li X, Chen Y, Hu W, Luo G N, Gao F and Deng H 2020 *Tungsten* **2** 3

[36] Liu L, Chen Y, Gao N, Liu Z, Gao F, Hu W and Deng H 2022 *J. Nucl. Mater.* **561** 153543

[37] Ziegler J F and Biersack J P 1985 *The Stopping and Range of Ions in Matter* (New York: Pergamon) **6** 93

[38] Nordlund K and Averback R S 1997 *Phys. Rev. B* **56** 2421

[39] Honeycutt J D and Andersen H C 1987 *J. Phys. Chem.* **91** 4950

[40] Stukowski A 2009 *Model. Simul. Mater. Sci. Eng.* **18** 015012

[41] Bai X M, Voter A F, Hoagland R G, Nastasi M and Uberuaga B P 2010 *Science* **327** 1631

[42] Tschopp M A, Horstemeyer M F, Gao F, Sun X and Khaleel M 2011 *Scripta Mater.* **64** 908

[43] Samaras M, Derlet P M, Van Swygenhoven H and Victoria M 2002 *Phys. Rev. Lett.* **88** 125505

[44] Liu L, Chen Y, Qiu R, Hu W and Deng H 2021 *Atomic Energy Science and Technology* **55** 8

[45] Björkas C, Nordlund K and Dudarev S 2009 *Nucl. Instrum. Meth. B* **267** 3204

[46] Juslin N, Jansson V and Nordlund K 2010 *Philos. Mag.* **90** 3581

[47] Fu B, Xu B, Lai W, Yuan Y, Xu H, Li C, Ji Y and Liu W 2013 *J. Nucl. Mater.* **441** 24